Available online at www.sciencedirect.com

ScienceDirect

Procedia Materials Science 9 (2015) 262 – 270

Procedia Materials Science

www.elsevier.com/locate/procedia

International Congress of Science and Technology of Metallurgy and Materials, SAM – CONAMET 2014

Study of the formation of Cu-24at.%Al by reactive milling

M. F. Giordana[a], N. Muñoz-Vásquez[b], M. Garro-González[c], M. R. Esquivel[a,d], E. Zelaya[a,*]

[a]*Centro Atómico Bariloche. CNEA-CONICET Av. Bustillo km 9.5. Bariloche, 8400, Argentina*
[b]*Instituto Balseiro (ANPCyT), Centro Atómico Bariloche, Av. Bustillo 9500, Bariloche 8400, Argentina*
[c]*Universidad Nacional de Costa Rica, POLIUNA. Avenida 1, Calle 9. Heredia, 86-3000, Costa Rica*
[d]*Centro Regional Universitario Bariloche – Universidad Nacional del Comahue. Bariloche, 8400, Argentina*

Abstract

In this work, powders of Cu and Al were milled with a proportion equal to 24 % atomic Al, using low and medium energy mills. The initial, intermediate and final stages of the resulting powder are analyzed using scanning electron microscopy, X-ray diffraction and different transmission electron microscopy techniques. The structure and microstructure achieved in each step of the milling process are compared to the results of Cu-16at.% Al and Cu-30at.%Al obtained under the same conditions of reactive milling. At the final stage of milling, it was detected that the obtained intermetallic is not the equilibrium phase of the Cu-Al system.

Peer-review under responsibility of the Scientific Committee of SAM–CONAMET 2014

Keywords: Reactive milling; Cu-Al; X-ray diffraction; scaning electron microscopy; transmission electron microscopy

1. Introduction

Cu-Al based shape memory alloys are appreciated due to the high transformation temperature, usually equal or higher than 200 ºC according to Dvorack (1983). The martensitic transformation gives rise to shape memory effect, pseudoelasticity and double shape memory effect (Ahlers (1986)). This transformation can be induced by a change of temperature or by the application of stresses and it is also independent of grains size within certain ranges.

* Corresponding author. Tel.: 0054 294 4445100 int 5548; fax: 0054 294 4445147.
E-mail address: zelaya@cab.cnea.gov.ar

Peer-review under responsibility of the Scientific Committee of SAM–CONAMET 2014
doi:10.1016/j.mspro.2015.04.033

However, the fracture strain seems to increase as the grain size decreases. Then, it is desirable to find a method to produce Cu-Al-Ni or Cu-Al shape memory alloys with a grain size lower than 30 μm according to Vajpai et al. (2011). There are several methods to produce microstructure alloys such as sputtering, argon atomization or addition of grain refiners like Zr or Ti. However, reactive milling (RM) is a useful tool recently incorporated as the first step in the synthesis of microstructural materials (Pourkhorshidi et al. (2012), Tang et al. (1997)). Moreover, the powders produced by reactive milling seem to favor the cohesion in the successive compaction stages due to the irregular shape. However, the equilibrium phases resulting from RM not always reproduce the results of the conventional phase diagrams. Depending on milling conditions, RM is a process that occurs near room temperature and involves the creation of phases due to repetitive fracture and rewelding of the powder particles inside a ball mill. Previous works in systems like Cu-Zn, Ni-Al or Ag-Zn showed evidence that the phase stability obtained by RM was different from the one obtained by conventional methods (Pabi and Murty (1996), Zelaya et al. (2013), Guzman et al. (2013)). In particular in Cu-Zn, it is shown that the discrepancies could be found in more than one specific composition value. For this reason, it is worth to study Cu-24at.%Al, even when the phase stability and microstructure of Cu-30at.%Al and Cu-16at.%Al were previously investigated

In the conventional phase diagram for Cu-16at.%Al, it is expected to found the cubic disordered α phase (Dvorack et al. (1983), Masalski et al. (1986)). This phase presents the same space group than Cu but with a slightly larger lattice parameter due to the Cu substitutional replacement by a larger Al atom (Swann and Warlimont (1963)). For higher Al concentrations, around Cu-24at.%Al the stable phase is the tetragonal α_2 (Swann and Warlimont (1963), Roulin and Duval (1997)). At Cu-30at.%Al, the phase diagram indicates the coexistence of the α_2 structure with the cubic γ_2 phase. This phase has a total of 52 atoms and 2 structural vacancies with a lattice parameter larger than three times the one of α. However, low energy RM of Cu-30at.%Al reaches mainly γ_2 phase while medium energy RM reaches an equilibrium between α and γ_2 phase. On the contrary, both types of RM seems to arrive to α phase for Cu-16at.%Al. This last result is in agree with the conventional phase diagram while Cu-30at.%Al is not (Giordana et al. (2014)).

The main purpose of this work is to fully characterize the structure, the microstructure and the phase stability of Cu-24at%Al obtained by low and medium energy ball mills. The powders were analyzed using, scanning electron microscopy (SEM), X-ray diffraction (XRD) and transmission electron microscopy (TEM). SEM was used in order to determine the evolution of the microstructure. The combination of XRD and TEM allows the proper study of the evolution of the phases with larger amount of mass and the detection with a threshold better than 1 nm the presence of minor phases in the final intermetallics. Finally, those results were compared with the evolution of Cu-16at.%Al and Cu-30at.%Al obtained by low and medium energy ball mills.

2. Experimental

Copper (99.999% purity) and aluminum (99.999% purity) powders were combined in a ratio of Cu–24at.%Al using two different ball mills. The elemental blends were mechanically alloyed in a horizontally-motioned mill Uniball Mill II-Australian Instruments. It is considered as a low-energy milling device (LEM) by Suryanarayana (2001) and Obregón et al. (2012). The elemental blends were also mechanically alloyed in a planetary-motioned mill Fritsch pulverissette 6, which is considered as a medium-energy milling device (MEM) by Suryanarayana (2001), Kano et al. (2000) and Lee (2012) .The milling processing and sample handling was done under Ar atmosphere (99.999%) at controlled conditions (humidity < 100 ppm, O_2 content < 5 ppm). Milling speeds selected were 140 rpm for LEM and 120 rpm for MEM. The ball/sample mass ratio for LEM was chosen as 22.33:1 and for MEM the ratio was equal to 8.25:1. After certain intervals of time, samples were withdrawn from the chamber by keeping approximately the same ball/mass ratio for XRD and TEM analysis. For LEM, the integrated milling times (t_{im}) selected were 10, 30, 50 and 100 hours and for MEM, the t_{im} were 10, 20, 30 and 50 hours. Table 1 presents the nomenclature used for the different samples.

Room temperature XRD was performed on a Philips PW 1710/01 Instrument with Cu K_a radiation. XRD patterns were refined by the Rietveld method using Fullprof software (Rodriguez Carvajal, (2001)). SEM images were acquired in an FEI 515. TEM characterization was performed using a FEI CM200UT microscope operated at 200 keV.

3. Results

3.1. SEM observations

The evolution of the mean sizes of the particles is summarized in Table 1.

Table 1. Type of mill and milling time employed for each sample and general characteristics of SEM and TEM measurements.

Sample name	Type of milling	Time of milling (h)	Mean particle diameter (μm)	Mean grain size (nm)
LCu24Al1	LEM	10	104 ± 43	5-35
LCu24Al2	LEM	30	122 ± 35	20-100
LCu24Al3	LEM	50	111 ± 31	15-100
LCu24Al4	LEM	100	99 ± 37	1-25
MCu24Al1	MEM	10	91 ± 38	6-50
MCu24Al2	MEM	20	101 ± 31	5-80
MCu24Al3	MEM	30	64 ± 23	4-80
MCu24Al4	MEM	50	60 ± 46	3-32

Moreover, the change in the morphology of the particles as time evolved is shown in Fig. 1. The initial stages of both milling types showed compact particles with a surface texture typical of fracture and cold welding processing of the powders. The last stage of milling of the low energy ball mill showed lenticular shape particles with some flats surfaces. On the contrary, the last stage of medium energy ball mill evidenced rounded particles with the same kind of surface of the MCu24Al1 sample. In order to compare the evolution of the mean size of the particles, the histograms of the initial and final t_{im} of each type of milling are shown together in Fig. 2. These results are also summarized with those of the samples analyzed in this work in Table 1. The normal curves of the histograms of samples Cu-30%at.Al and Cu-16%at.Al are also plotted together with the histograms of Cu-24%at.Al for the same time of milling and type of mill.

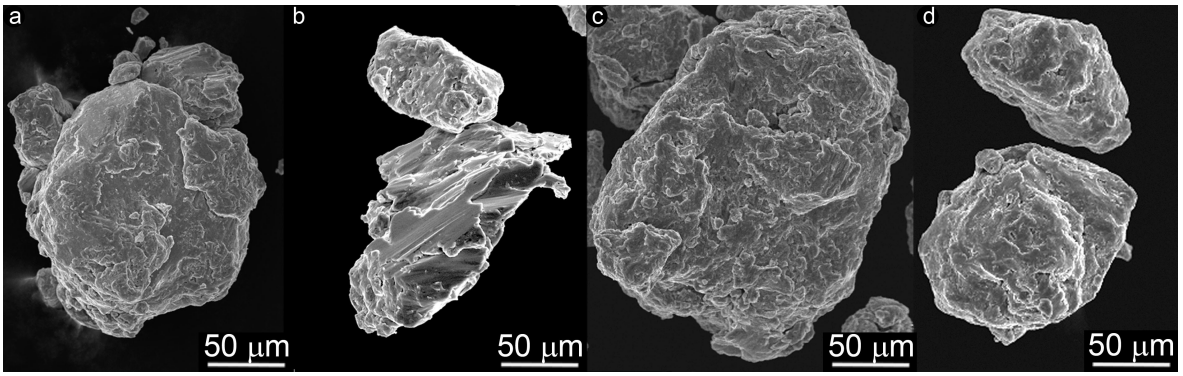

Fig. 1. SEM micrographs with the same magnification of samples (a) LCu24Al1, (b) LCu24Al4, (c) MCu24Al1, (d) MCu24Al4.

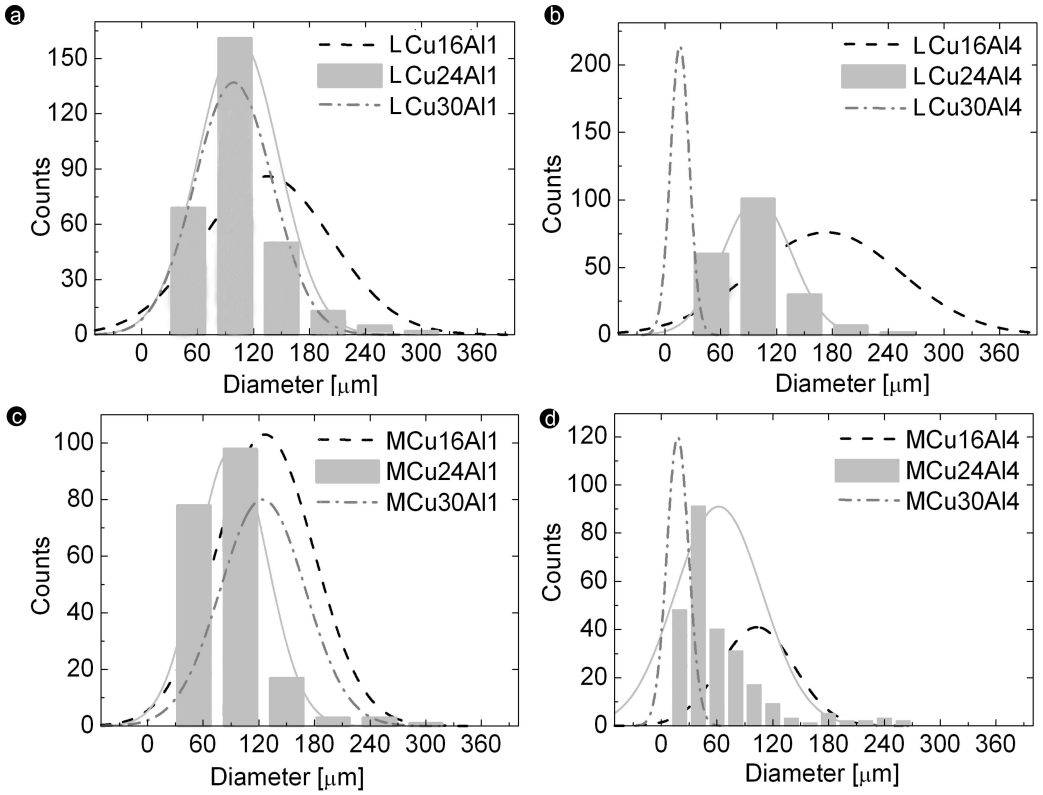

Fig 2. Histograms and fitting of normal curves in light gray of samples (a) LCu24Al1, (b) LCu24Al4, (c) MCu24Al1, (d) MCu24Al4. Each figure shows the normal fit to the samples Cu-16%atAl in dash black lines and Cu-30%atAl in dot dash dark gray lines for the exact milling time and mill type.

As it can be observed in Fig. 2, the discrepancies between the main values of the normal curves associated to the histograms at the initial integrated milling times are lower than 60 μm. However, a slight tendency to decrease the mean diameter as the Al% increases could be mainly detected in Fig. 2(a). At the longest t_{im}, the mean size diameter of the particles clearly decreased as the amount of Al increases (Figs. 2(b) and (d)).

3.2. TEM observations

Fig. 3 shows the typical dark field image of the milled particles. This kind of microstructure was observed in all the samples. The ranges of the grains measured from the dark field images are summarized in Table 1.

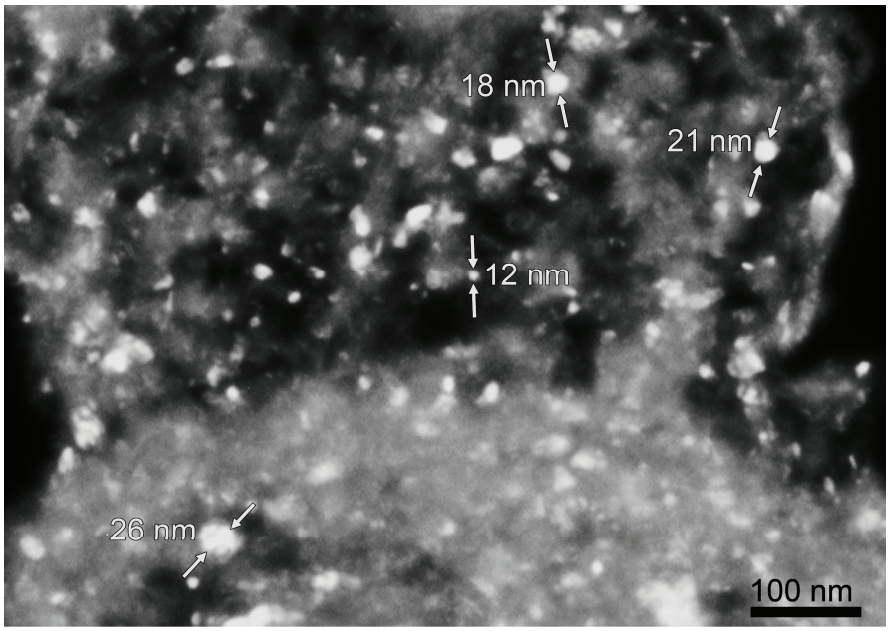

Fig 3. Dark field image of the sample LCu24Al1.

Fig. 4(a) shows one of the typical left up quarter of the ring diffraction pattern. As it is observed in Fig. 4(b), indexing phase exhibited a linear correlation between the measured data and those obtained considering a lattice parameter equal to 0.364 nm (Pearson, (1958)). Even when only one other possibility (γ_2 phase) was analyzed in this figure, no other phase of the equilibrium phase diagram between Cu-16at.%Al and Cu-30%at.Al fit as good as the α phase in this case. However, most of the ring diffraction patterns of the samples analyzed in this work matched with more than one phase. Figs. 4(c) and (d) show typical examples of the left up quarter of initial and final stages of milling. The association of the indexation of each ring diffraction pattern is listed in Table 2, no particular rings associated to other phases rather than α and γ_2 could be detected in the intermediate and final t_{im}. However, a certain tendency to show completed α rings and incomplete γ_2 (like in Fig. 4(d)) was more frequent in low energy mill samples. Moreover, only in samples MCu24Al2 and MCu24Al3 some of the particles presented a ring diffraction pattern consistent with the presence of α phase (Fig. 4(b)).

Table 2. Indexed phases according TEM and XRD techniques.

Sample name	TEM	XRD
LCu24Al1	Cu + Al	Cu + Al
LCu24Al2	$\alpha + \gamma_2$	$\alpha + \gamma_2$
LCu24Al3	$\alpha + \gamma_2$	$\alpha + \gamma_2$
LCu24Al4	$\alpha + \gamma_2$	$\alpha + \gamma_2$
MCu24Al1	Cu + Al	Cu + Al
MCu24Al2	$\alpha + \gamma_2$	$\alpha + \gamma_2$
MCu24Al3	$\alpha + \gamma_2$	$\alpha + \gamma_2$
MCu24Al4	$\alpha + \gamma_2$	$\alpha + \gamma_2$

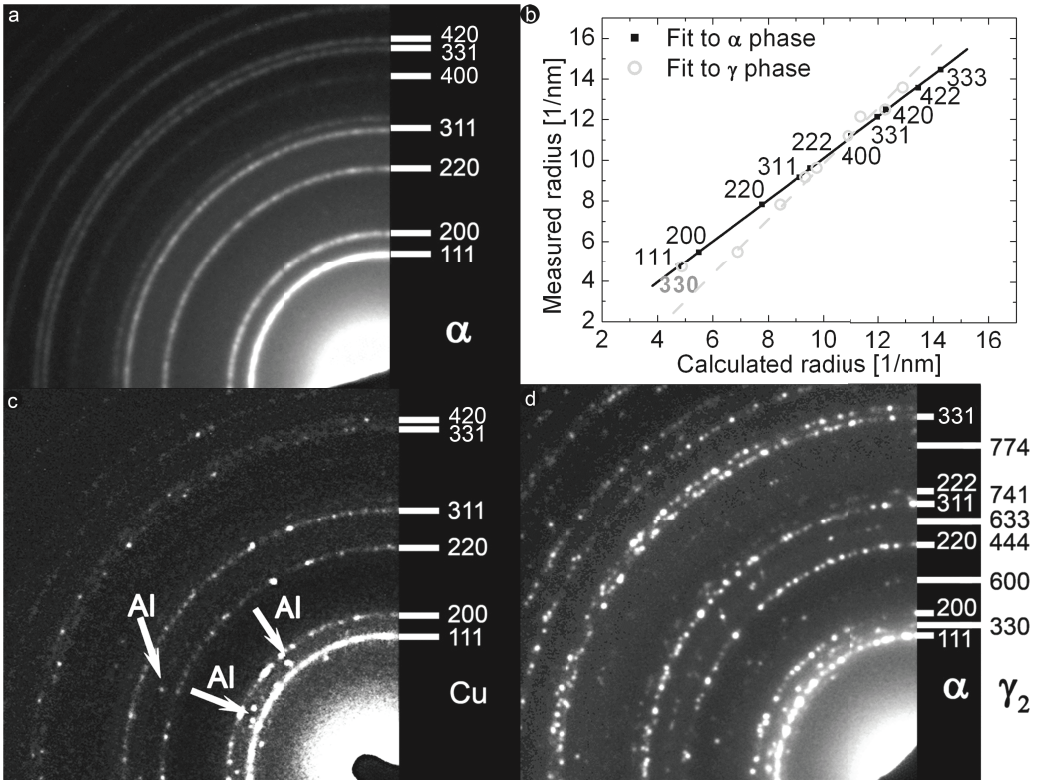

Fig 4. (a) Left up ring diffraction pattern of sample MCu24Al3, (b) Diameter of the rigs measured in (a) as a function of the diameter of α and γ_2 phases, (c) Left up ring diffraction pattern of sample LCu24Al1, (d) Left up ring diffraction pattern of sample MCu24Al4.

3.3. X-Ray diffraction patterns

The diffractograms of the intermediate and final stages of the milling could be indexed consistently with the presence of only α and γ_2 phases (Table 2). However, two different types of profiles were observed for the low and medium RM. In all LCu24Al2, LCu24Al3 and LCu24Al4 samples the peak corresponding to $330_{\gamma 2}$ at $2\theta = 44^{\circ}$ could be clearly distinguished from the peak corresponding to 111_{α} at $2\theta = 42.8^{\circ}$ (detail in Fig. 5(a)). On the contrary, in samples MCu24Al2, MCu24Al3 and MCu24Al2 the peak indexed as $330_{\gamma 2}$ appears as a very low shoulder of 111_{α} (detail in Fig. 5(b)). This behavior could not be attributed to texture of the samples since neither ring diffraction pattern nor dark field images showed characteristics of textured samples.

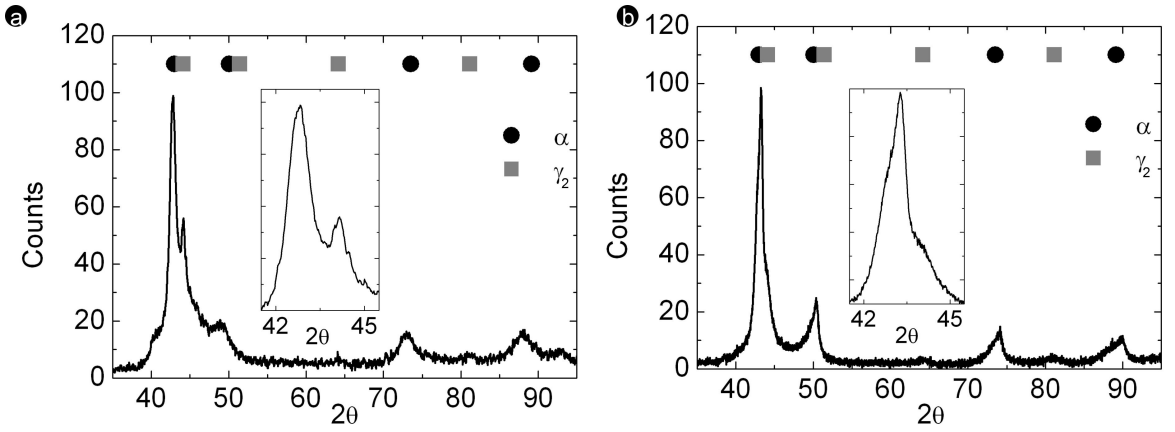

Fig 5. (a) Diffractogram of sample LCu24Al4, (b) Diffractogram of sample MCu24Al4.

Finally, Table 3 presents the results of the average grain size calculated with Scherrer formula for the first and last t_{im}, considering the width at half peak height in the peaks of each diffractogram. Those values are within the range observed in the dark field images and listed in Table 1.

Table 3. Variation of grain size according the type and integrated time of milling. The technique has an error of ± 1 nm to determine grain size.

Diffraction	LCu24Al1	LCu24Al4	MCu24Al1	MCu24Al4
phase	Cu	α	Cu	α
(111)	20 nm	50 nm	–––	12 nm
(200)	21 nm	37 nm	–––	10 nm
(220)	22 nm	29 nm	8 nm	12 nm
(311)	17 nm	26 nm	10 nm	10 nm

4. Discussion

The particles obtained by LEM were less rounded than the ones resulted by MEM. This behavior was also reported for Cu-16at%Al and Cu-30at.%Al (Giordana et al. (2015)) and it is associated to the movement of the balls inside the milling vessel. While in LEM the balls hit the material and the chamber in one vertical movement, in MEM the impacts come from randomly distributed directions. In other words, the shape of the particles seems to be determined by the type of movements of the balls inside the chamber.

All the particles obtained for the first integrated milling time showed the same kind of surfaces. They looked like lamellar material welded one over each other. This kind of microstructure could be associated to multiple fractures and cold welding processes. Even when the initial integrated milling times are short, the fracture of the pure Cu and Al particles occurred. However, the analysis of the diffractograms and the ring diffraction patterns are both consistent with the presence of Cu and Al. Neither technique detected the presence of the intermetallic. Therefore, each particle in the first t_{im} is formed of pure Cu and Al grains.

As the milling time increased, the mean size of the particles decreased (Table 1). At the same time, the diffractograms and the ring diffraction patterns showed the consolidation of α and γ_2 phases. For t_{im} longer than 30 hours in LEM and 20 hours in MEM, the successive fracture and rewelding of the particles activate the formation of the intermetallics. The mean particle sizes of the longest t_{im} analyzed in this work had values between the ones obtained for the same t_{im} in Cu-16at%Al and Cu-30at.%Al (Fig. 2 and Giordana et al. (2015)). It is worth to mention that for LEM only α phase was obtained after 100 hour of milling of Cu-16at.%Al while only γ_2 phase was obtained after 100 hour of milling of Cu-30at.%Al (Giordana et al. (2014)). In this work, a mixture of α and γ_2 phases was detected as the final intermetallic. Therefore, the decrement of the particle size as the Al content increases could be attributed to the increment of the γ_2, since this phase is much more fragile than the α one.

The grain size obtained due to an indirect type of calculation (Table 3) was in agreement with the grain sizes observed by TEM (Fig. 3). However, no significant evolution was observed in neither of the different t_{im}. The same behavior was observed in this system for Cu-16at%Al and Cu-30at.%Al (Giordana et al. (2015)). However, in other systems, like Ni-35at.%Al, it was observed a decrement of grain size as the milling time increases (Zelaya et al. (2013)). The lack of grain size evolution of Cu-Al could be associated to an absence of high energy movement of defects easily activated by milling processes.

For t_{im} longer than 20 hours only α and γ_2 phases were detected. Taking into account the total intensity of the rings of the diffractions patterns (Fig. 4) and the height of the peaks associated to each phase in the diffractograms (Fig. 5), the amount of γ_2 phase seemed larger for LEM. The same behavior was observed using the same type of mills in Cu-30at.%Al (Giordana et al. (2014)). In that work, it was found that the phase formation for those system formed at first the α phase (isostructural with Cu) and after that process, the formation of γ_2 took place. Assuming that idea, the LEM seems to be more efficient than the MEM in terms of consumed time to arrive to a final asymptotic stage of milling.

Finally, it should be mentioned that neither by LEM nor by MEM the equilibrium phases were in agree with the phase diagram. At Cu-24at.%Al the phase diagram showed a boundary between α_2 and γ_2 phases. The lack of coincidence between the phases achieved by RM and conventional method was already observed in this and other systems (Guzman et al. (2013), Pabi et al. (1996), Zelaya et al (2013) and Giordana et al. (2014)). The synthesis of intermetallics by RM at room temperature is associated to diffusion processes rather than to nucleation and growth of phases. For this reason the alloys generated by RM were different than the ones produced by conventional melting methods.

5. Conclusion

The formation of the intermetallic by low and medium energy ball mill was detected for Cu-24at.%Al.

The mean particle size of Cu-24at%Al was larger than Cu-16at%Al and smaller than Cu-30at%Al at the final stages of milling.

The mean size of the grains did not present a large variation as the milling time evolves.

Both XRD and TEM techniques detected the presence of α and γ_2 phases at intermediate and final t_{im} of the milling.

The intermetallics obtained by both types of milling were not the equilibrium ones according the conventional phase diagrams.

Acknowledgements

The authors express their thanks to Consejo Nacional de Investigaciones Científicas y Técnicas (CONICET), to Agencia Nacional de Promoción Científica y Tecnológica (ANPCyT: PICT-2011-0643 and PICT-2011-0092) and to Comisión Nacional de Energía Atómica (CNEA) for supporting this work.

References

Ahlers M., 1986, Martensite and equilibrium phases in Cu-Zn and Cu-Zn-Al alloys; Progr. Mater. Sci. 30, 135-186.

Dvorack M.A., Kuwano N., Polat S., Haydn Chen, Wayman C.M., 1983, Decomposition of a β1-phase Cu-Al−Ni alloy at elevated temperature, Scripta Metallurgica Vol. 17, 1333-1336.

Giordana M.F., Esquivel M.R., Zelaya E., 2014, A detailed study of phase evolution in Cu-16 at.%Al and Cu-30 at.%Al alloys under different types of mechanical alloying processes, Advanced powder technology, in press.

Giordana M.F., Muñoz-Vasquez N., Esquivel M.R., Zelaya E., 2015, Microstructure evolution of Cu-16 at.%Al and Cu-30 at.%Al alloys under different types of mechanical alloying processes, unpublished results.

Guzmán D., Rivera O., Aguilar C., Ordoñez S., Martínez C., Serafini D., Rojas P., 2013, Mechanical alloying and subsequent heat treatment of Ag–Zn powders, Trans Nonferrous Met Soc China, 23, 2071−2078.

Kano J., Miyazaki M., Saito F., 2000. Ball mill simulation and powder characteristics of ground talc in various types of mill, Adv Powder Technol, 11(3), 333–342.

Lee J., 2012, Grinding effects on the change of particle properties in cupric sulfide, CuS, Adv Powder Technol, 23(6), 731–735.

Massalski T.B., Murray J.L., Bennett L.H., Baker H., 1986, Binary Alloy Phase Diagrams, Vol 1 and 2, American Society for Metals, Metals Park, OH..

Obregón S.A., Andrade Gamboa J.J., Esquivel M.R., 2012. Synthesis of Al-containing MmNi5 by mechanical alloying: milling stages, structure parameters and thermal annealing, Int J Hydrogen Energy, 37(19), 14972-14977.

Pabi S.K., Murty B.S., 1996, Mechanism of mechanical alloying in Nisingle bondAl and Cusingle bondZn systems, Mater. Sci. Eng. A214, 146-152.

Pearson W. B., 1958, A Handbook of Lattice Spacings and Structure of Metals and Alloys, Pergamon Press, NewYork.

Pourkhorshidi S., Parvin N., Kenevisi M.S., Naeimi M., Ebrahimnia Khaniki H., 2012, A study on the microstructure and properties of Cu-based shape memory alloy produced by hot extrusion of mechanically alloyed powders, Materials Science& Engineering A 556, 658-663.

Roulin G., Duval P., 1997, Initial stages of ordering obtained by tempering of disorder martensitic phase of Cu-Al alloys, Scr Mater, 37, 45-51.

Rodriguez-Carvajal, J., 2001. Recent developments of the program FULLPROF, Comm. Powder Diffr. (IUCr) 26, 12-19.

Suryanarayana C., 2001. Mechanical alloying and milling, Prog Mater Sci, 46, 1-184.

Swann P.R., Warlimont H., 1963, The electron-metallography and crystallography of copper-aluminum martensites, Acta Metall, 11(6), 511-527.

Tang S.M., Chung C.Y., Liu W.G., 1997, Preparation of Cu-Al-Ni-based shape memory alloys by mechanical alloying and powder metallurgy method. Journal of Materials Processing Technology, 63, 307-312.

Vajpai S.K, Dube R.K., Sangal S., 2011, Microstructure and properties of Cu–Al–Ni shape memory alloy strips prepared via hot densification rolling of argon atomized powder perform, Materials Science and Engineering A 529, 378-387.

Zelaya E., Esquivel M.R., Schryvers D., 2013, Evolution of the phase stability of Ni–Al under low energy ball milling, Advanced Powder Technology 24, 1063–1069.